This is an author's version published in: http://oatao.univ-toulouse.fr/28843

Acoustic Emission Characterization of Transgranular Cracks in WC–Co Cemented Carbides During a One-way Scratch

M. Yahiaoui[1] · **M. Marconnet[1]** · **K. Jlaiel[1]** · **J.-Y. Paris[1]** · **J. Denape[1]**

Abstract

The tribological behavior of tungsten carbide–cobalt materials is influenced by the cobalt content and the WC grains size. The main wear mechanisms in these materials are cobalt depletion, intergranular cracks, and WC grain cleavages. More specifically, coarse WC grains favor the apparition of transgranular cracks during sliding friction tests. A promising way to access in real-time blinded tribological contacts is the technique of acoustic emission (AE). This study clearly identifies transgranular cracks in AE signals. The AE energy and frequency of this mechanism were experimentally associated with the size of the transgranular cracks. A mechanical model based on the classical beam theory and harmonic motion equations confirms these relations. The AE centroid period (i.e., inverse of the centroid frequency) increases linearly with the size of the transgranular cracks. The AE energy increases linearly with the cube of the transgranular cracks length.

Graphical Abstract
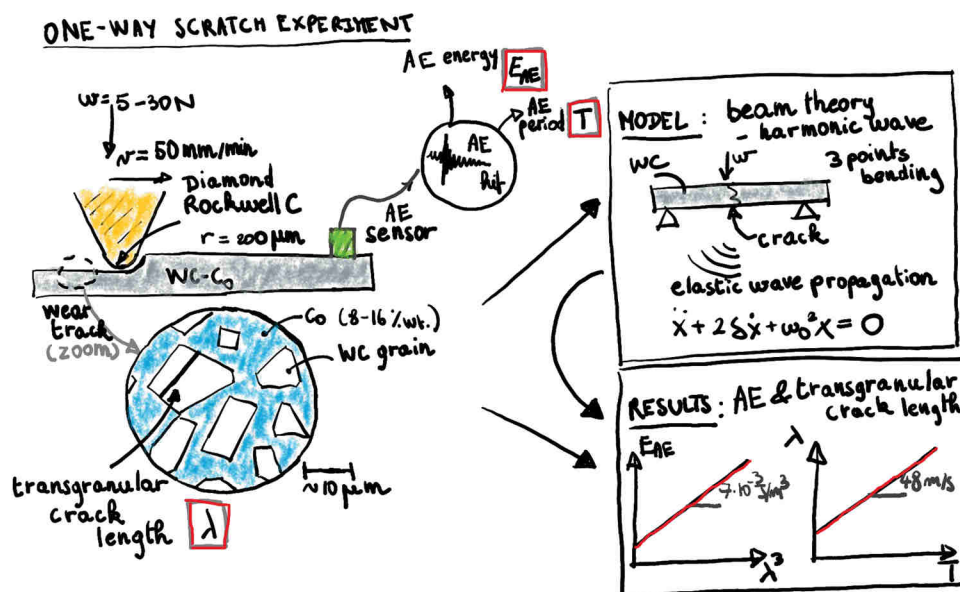
✉ M. Yahiaoui
malik.yahiaoui@enit.fr

1   Laboratoire Génie de Production, Université de Toulouse, École Nationale d'Ingénieurs de Tarbes, 47 avenue d'Azereix, 65000 Tarbes, France

1 Introduction

The wear mechanisms of tungsten carbide–cobalt WC–Co were broadly studied in the field of rock drilling and metal machining tools. Chermant and Osterstock [1] first described

that the wear of WC–Co is mainly caused by intergranular cracks in the cobalt binder phase. In addition, with cemented carbides with cobalt content between 3 and 20 wt%, the contiguity of WC aggregates produces transgranular cracks. The transgranular cracks occurrence increases with the WC grain size [2]. The depletion of cobalt by abrasive particles [3] is also an important tribological behavior acting on the interface rheology and contributing to a solid lubrication effect [2]. These mechanisms are usually characterized using post-mortem analyses of the worn surfaces. One way to access a blinded interface in real time is the use of the acoustic emission (AE) technique.

AE are transient mechanical waves (ultrasound) produced by the release of elastic energy from a default displacement in materials under stress. Baranov et al. [4] exposed different sources of AE, their dissipated energy, and frequency ranges in sliding contacts. In the literature, the AE results in tribology are often qualitative and are associated with the materials properties and complex wear mechanisms combining unidentified elementary mechanisms. For instance, Baranov et al. explained that a rough relief, a high hardness, and abrasive wear (e.g., cutting, plowing, or fragmentation by relatively sharp asperities) are factors of increase in AE amplitude. Conversely, fine grains, slow sliding velocity, and adhesive wear (e.g., detachment and transfer of material consecutive to an adhesive interaction and plastic deformations) are factors of decreasing amplitude of the AE signals. The review performed by Hase et al. [5] illustrates the difficulties to accurately associate AE signals to elementary wear mechanisms. They present a correlation map with large AE frequency bands linked to tribological phenomena blends. Sliding friction is located in a frequency band between 20 and 300 kHz [6]. Abrasive wear is associated to a 200 kHz–1 MHz band. Some severe wear and adhesive wear are found in a higher 1–1.5 MHz band. Different types of mechanical tests are also displayed on the map with tensile testing from 0 to 500 kHz and fatigue testing from 200 to 450 kHz [7]. Lately, Feng et al. [8] review on AE in tribology concludes that most of the previous studies are experimental and few works are presenting theoretical models. Actually, most of these studies propose qualitative relations among AE and operating parameters (e.g., load and velocity), materials
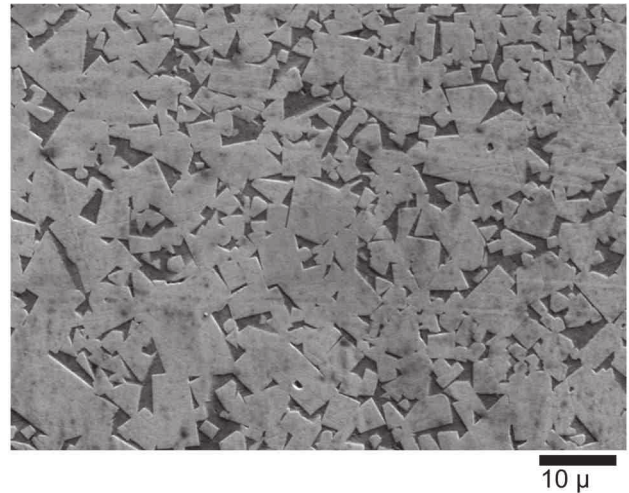
Fig. 1 SEM image of the P12's polished section: WC grains in gray and Co phase in black

properties (e.g., surface roughness), or tribological outputs (e.g., friction and wear).

This paper presents an experimental and theoretical approach focused on one elementary interfacial wear mechanism in cemented carbide: the transgranular crack. The aim of this study is to clearly associate AE events to this precise mechanism and to provide direct relations between AE signals and one AE source characteristic, i.e., the transgranular crack length.

2 Materials and Methods

2.1 WC–Co Samples

Three grades of WC–Co cemented carbide were studied: P8, P12, and P16 [2]. These carbides contain respectively 8 ± 1 wt%, 12 ± 2 wt% , and 15 ± 2 wt% of cobalt (Table 1).

The samples contain WC characteristic prismatic grain geometry surrounded by a cobalt binder phase (Fig. 1). The WC grain has similar values of apparent diameter (Feret diameter) and height [9]. The P8 and P16 samples have a monomodal grain size distribution with mean grain sizes of, respectively, 2.8 ± 1 μm and 5.0 ± 1.3 μm. The P12 has a bimodal grain size distribution with a mean grain size of 7 ± 3 μm. For this carbide, the two populations of grains are centered at 3.6 ± 0.4 μm and 5.6 ± 0.5 μm.

These three microstructures produce different mechanical properties. The cobalt content and the grain size directly act on the compromise between carbides hardness and resilience. For instance, smaller grains form harder carbides and higher cobalt content increases the fracture toughness [1, 10].

Table 1 WC–Co inserts physicochemical and mechanical properties

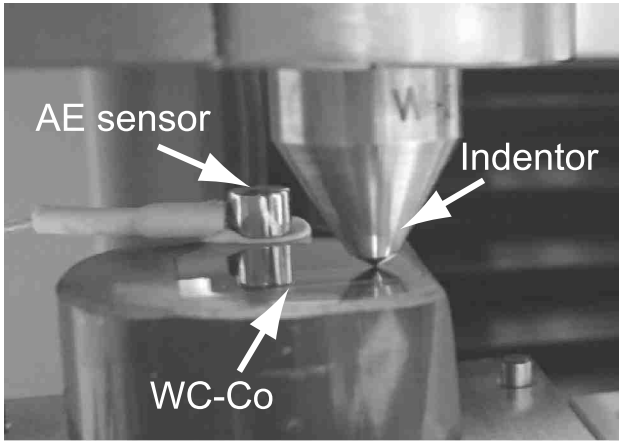| Insert	Cobalt content (wt%)	Average grain size (μm)	Density ±0.05 g/cm³	Young modulus (±10 MPa)	Hardness (HV 2 kg/10 s)
P8	8 ± 1	2.8 ± 1	15.03	594	1326 ± 21
P12	12 ± 2	7 ± 3	14.43	546	1095 ± 29
P16	15 ± 2	5.0 ± 1.3	14.03	502	1061 ± 3

Fig. 2 Rockwell C indentor/WC–Co contact setting

2.2 Experimental Procedure

A microscratch test device (CSM MST) was used as a linear tribometer with a Rockwell C indentor, i.e., spherical diamond tip with a radius of 200 μm (Fig. 2). Each test consisted in a one-way single scratch on WC–Co samples polished surface of 10 mm at a velocity of 50 mm/min. Three different normal loads were used at 5 N, 15 N, and 30 N. These loads correspond to initial maximum contact pressures ranged from 15 to 29 GPa certainly exceeding the yield stress of cemented carbides. Before testing, the WC–Co samples and the indentor were cleaned for 15 min using an industrial detergent, then rinsing with demineralized water, and finally 10 min ultrasonic cleaning with ethanol before drying at 60 °C for 15 min.

An AE sensor was coupled directly to the WC–Co surface using a water-based adhesive containing styrene acrylic copolymer. This sensor (Pico sensor from Euro Physical Acoustic) is a large band type operating at its maximum sensitivity between 100 kHz and 1 MHz. The distance between the sensor and the scratches varies between 0.5 and 1.5 cm depending on the position of the scratch. The distance between two consecutive scratches is about 500 μm. For a test condition, the scratches were repeated four times at different positions, and no sensor-scratch distance effect was detected.

2.3 Acoustic Emission Signals

During experiments, the acoustic emission signals, i.e., hits were sampled considering the parameters defined in Table 2. Two signal characteristics were considered: the absolute acoustic energy E_{AE} and the centroid frequency f_c [11]. The absolute acoustic energy is extracted by integrating the absolute value of the acquired hits over the sampling periods. The centroid frequency represents the frequency center of mass of the acoustic emission signals, and it characterizes the overall frequency content of an acoustic emission signal. These parameters are used to follow any significant changes in the sliding contact behavior and to complete the mechanical information given by the friction coefficient.

3 Results

3.1 Friction and Wear Results

All experiments have a steady friction along the single scratch after a quick increase during the contact setting (Fig. 3a). The P8 and P16 samples display the same friction coefficient of 0.19 (Amontons–Coulomb law fits, Fig. 3b).

Table 2 Acquisition parameters of acoustic emission signals with the peak definition time (PDT), the hit definition time (HDT), and the hit lockout time (HLT)

Threshold (dB)	Preamplification (dB)	Sample rate (MHz)	Pre-trigger	PDT (μs)	HDT (μs)	HLT (μs)
30	40	5	50	1000	2000	20,000

Fig. 3 Friction results: **a** Friction coefficient vs. travel distance with the P12 sample at a load of 30 N; **b** Transverse force vs. normal load with Amontons–Coulomb law fits
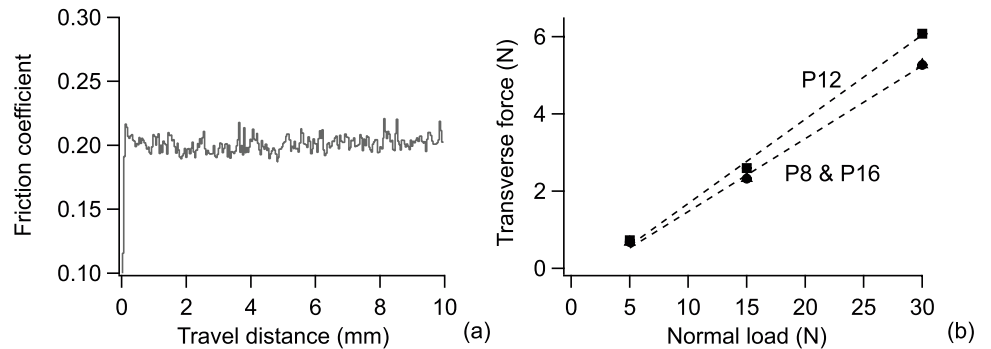
The P12 has a slightly higher friction coefficient of 0.22. These results imply that the WC grain size influences the friction and that the cobalt content does not change the friction amplitude. At the lowest load of 5 N, all the samples reach the same value of friction.

During scratch tests, the main WC–Co material displacement is produced by plastic deformation. The scratch transverse profile shows a good conformity with the Rockwell C indentor with small plastic beads formed on the edges (Fig. 4a). Consequently, the wear height h is proportional to the load w (Fig. 4b), with the linear wear rate k corresponding to the proportionality coefficient (Fig. 4c). The cohesive wear volume V can then be directly calculated from the indentor geometry and the hardness H of the carbide samples (with L the scratch length and R the indentor radius) (Eq. 1).

$$\begin{cases} V = R^2 L \left[\arccos\left(1 - \frac{h}{R}\right) - \left(1 - \frac{h}{R}\right)\sqrt{1 - \left(1 - \frac{h}{R}\right)^2} \right] \\ \quad + \frac{\pi}{3}h^2(3R - h) \\ h = k \cdot w = [(-0.119 \pm 0.005) \cdot H + (224 \pm 6)] \cdot w \end{cases}$$

$$(1)$$

## 3.2 Interfacial Wear Mechanisms

The observed interfacial mechanisms are similar to the WC–Co wear mechanisms described in the literature (Fig. 5):

– Cobalt extraction from the cemented carbide flowing into the interface (mainly with P8 and P16 samples).
– Intergranular cracks are mainly observed on the scratch edges around the plastic beads but also in the track.
– Coarse grains plastic deformation by crystallographic sliding planes (mainly with P12 samples).
– Transgranular cracks are clearly observed in the track (mainly with P12 samples).

These observations give a clear explanation on the friction coefficient similarity between P8 and P16. The lower WC grain size of the P8 and P16 samples appears to induce a higher cobalt binder extraction during tests. In a third body point of view, this cobalt extraction feeds, through the source flow, the interface. In this way, a solid lubrication mechanism occurs at the interface and lowers friction by a shearing mechanism of the third body. At low loads, the contact pressure seems to be not enough to extract cobalt from the WC–Co microstructure avoiding the solid lubrication mechanism. This explains the similar friction reached by all samples at lower loads.

At the interface, transgranular cracks are the most energetic mechanical dissipation mechanisms. These cracks are mainly observed in the P12 sample, which has the coarsest grains, followed by the P16 (Fig. 6a). the cracks count also increases with the load. The transgranular cracks count follows the grain size distributions (Fig. 6b) and the maximum cracks count is reached around the grain size medians. In this way, for the P12, the cracks count follows the grain size

Fig. 4 Cohesive wear mechanism: **a** Optical interferometer measurements; **b** Wear height vs. load; **c** Linear wear rate vs. hardness
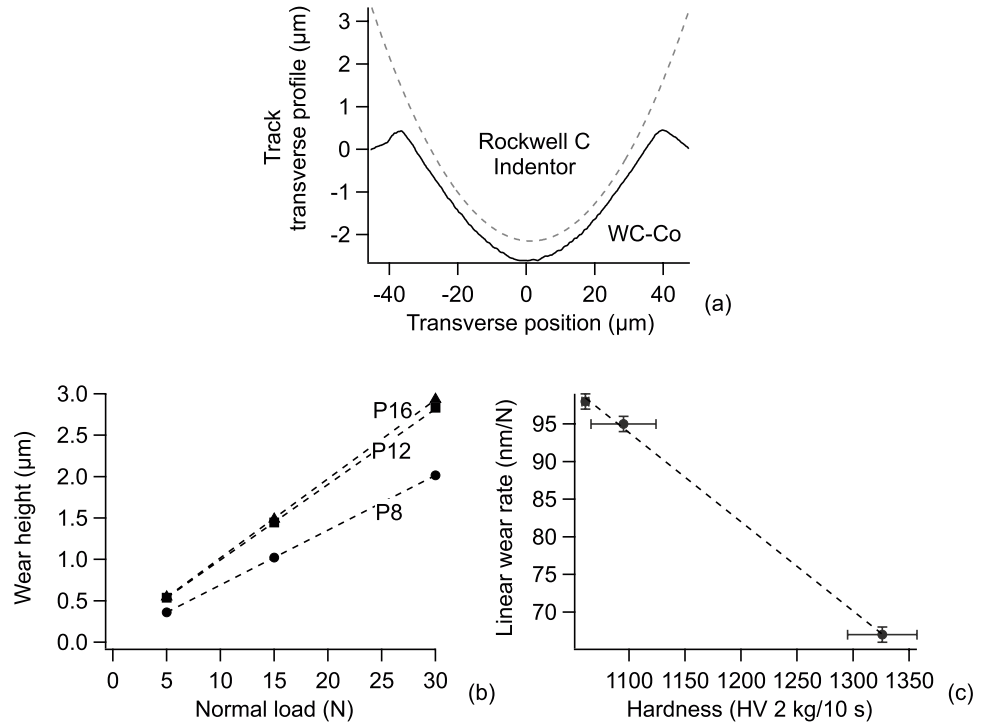
Fig. 5 SEM images of scratches on P8, P12, and P16 samples after tests at 30 N with intergranular cracks (white cracks around grains), transgranular cracks (cleavages in the grains), grains plastic deformation (visible plane sliding in the grains), and cobalt extraction (longitudinal black trails)
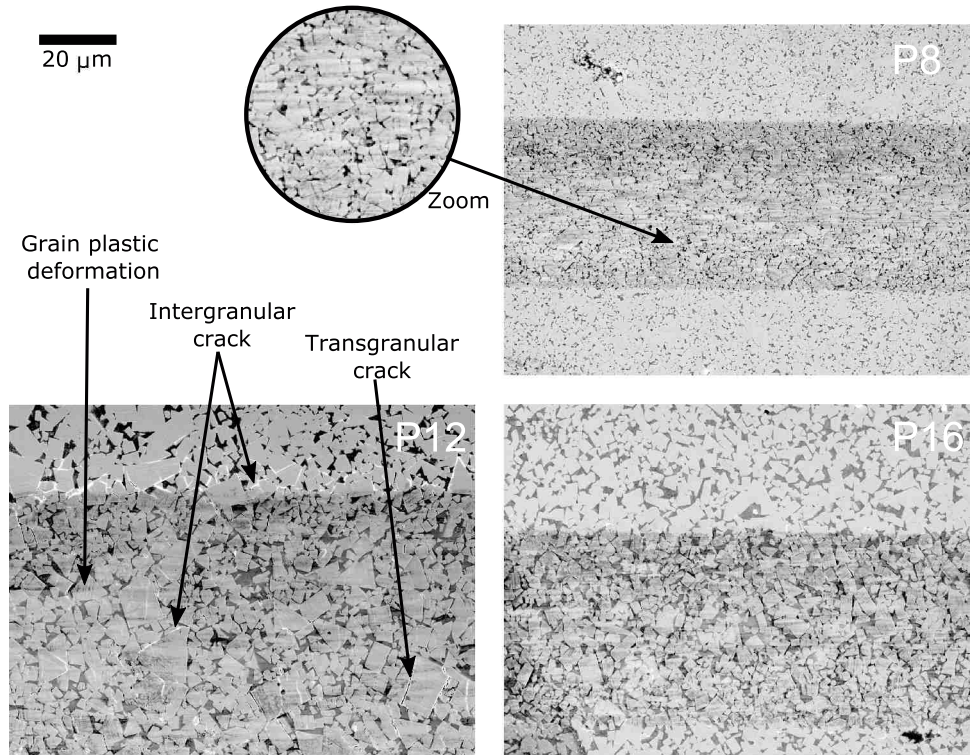
Fig. 6 Transgranular cracks statistics: **a** Cracks count in the track; **b** cracks count distribution over the WC grain size; **c** cracks length vs. grain size and linear fit with a coefficient of determination of $R^2 = 99\,\%$
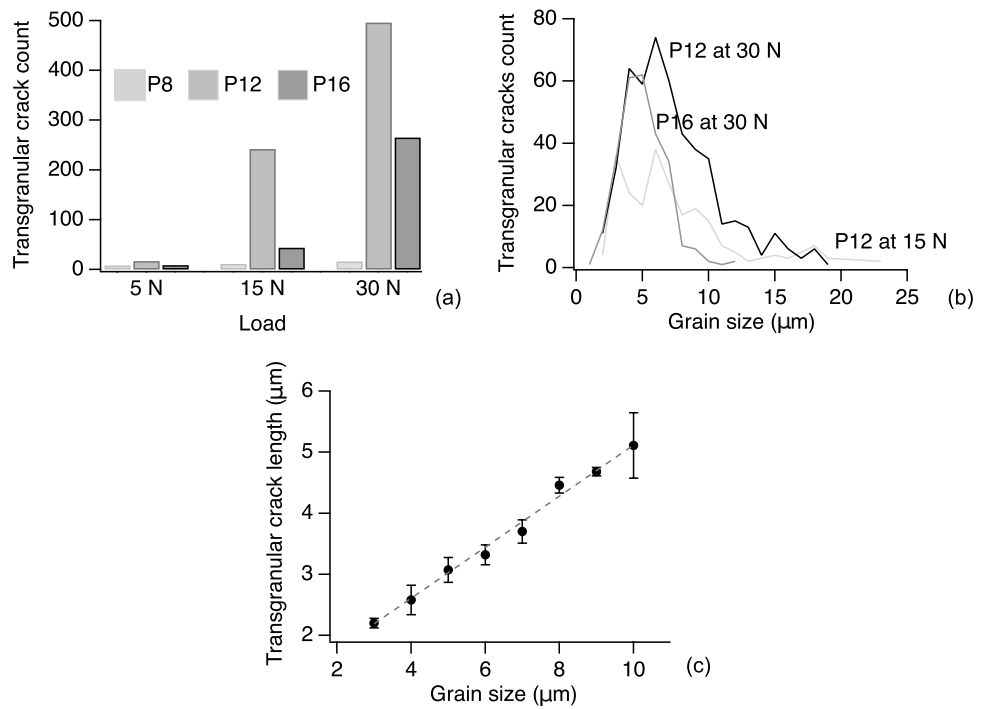
bimodal distribution with two peaks around 4 μm and 6 μm. The minimum and maximum cleaved grain size observed are, respectively, about 1 μm and 23 μm.

Furthermore, the transgranular cracks are perpendicular to the sliding direction with a mean angle of $92° \pm 16°$. The transgranular cracks length λ is perfectly related to the cleaved grains size d (Feret diameter) with the linear relation 2 (Fig. 6c). The minimum and maximum observable cracks lengths are then, respectively, about 0.5 μm and 10 μm.

$$\lambda = (0.42 \pm 0.02) \cdot d + (0.9 \pm 0.2) \cdot 10^{-7}. \tag{2}$$

3.3 Acoustic Emission Correlations

The acoustic emission-acquired signals are mostly coming from transgranular cracks produced during the tests. Fig. 7a displays the similarity between the AE absolute energy evolution and the transgranular cracks length measured over the scratch. As multiple cracks can be observed on one grain or simultaneously on the scratch, a cumulative transgranular cracks length λ at a position on the

scratch was then considered. In this way, the first correlation is that the AE absolute energy E_{AE} increases with the cumulative transgranular crack length (Fig. 7b) following a degree 3 polynomial function (Eq. 3). The associated AE absolute energy lower and upper limits are then, respectively, about 0.62 aJ and 7.62 aJ.

$$E_{AE} = (7.0 \pm 0.4) \cdot 10^{-3} \cdot \lambda^3 + (6.2 \pm 0.3) \cdot 10^{-19}. \tag{3}$$

The second correlation is that the cumulative transgranular cracks length increases linearly with the AE centroid period T (i.e., the inverse of the AE centroid frequency) (Fig. 7c, Eq. 4). This relation implies that the centroid frequency band for WC transgranular cracks spreads between 578 kHz and 658 kHz.

$$\lambda = (48 \pm 2) \cdot T - (7.3 \pm 0.3) \cdot 10^{-5} \tag{4}$$

The slope of λ vs. T relation is a characteristic of the WC grain cleavage. It could represent the crack velocity of the grain performed at 48 ± 2 m/s. This hypothesis is not verified in this study, but similar ranges of crack velocity in polycrystalline ceramics is exposed in the literature [12, 13].

Fig. 7 Acoustic emission correlated with transgranular crack length (P12 sample at 15 N over a scratch portion of 500 μm): **a** absolute energy and cumulative transgranular cracks length vs. position on scratch; **b** absolute energy vs. the cube of the cumulative transgranular cracks length ($R^2 = 98$ %); **c** centroid period vs. cumulative transgranular cracks length ($R^2 = 95$ %)
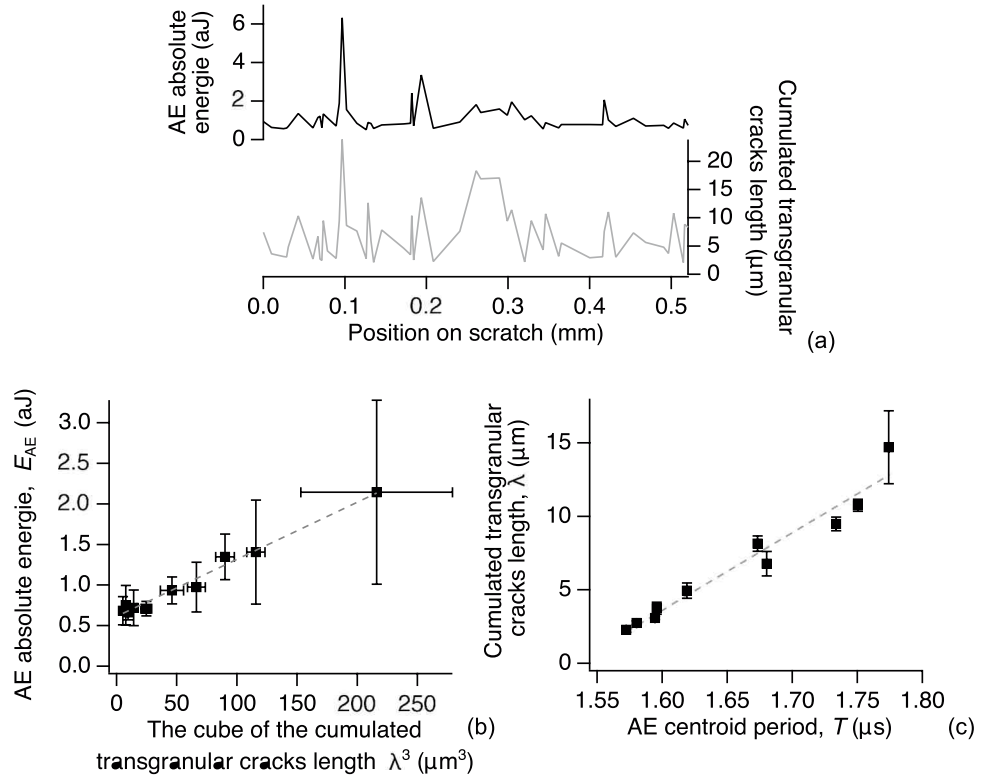
4 Discussion

A simple mechanical wave harmonic model associated with a classical beam theory is applied to illustrate the physics behind the direct relation between WC transgranular cracks length and the acoustic emission parameter of centroid period. Because of the WC grains contiguity in the cemented carbide considered here, a central three-point bending model is applied to a WC grain in first approximation. This approach is supported by the observations of the cracks perpendicular to the sliding direction and by the cleavages formed near the middle of a grain. When the grain is bent and reaches its ultimate deformation, the transgranular crack propagates. The grain splits, the two parts of the grain vibrate and release free oscillations generating an elastic mechanical wave. Only a small part of this wave is acquired by the acoustic emission device. Equation 5 uses the damped simple harmonic motion model with the natural frequency ω_0 calculated from the ratio between the WC grain stiffness k and its mass m (the WC grain geometry is approximate to a cylinder of apparent diameter and height equal to d). The centroid frequency can then be calculated from the angular frequency: $f_c = \frac{\omega}{2\pi}$. The damping ratio ζ is given by the ratio between the damping coefficient δ and the natural frequency. As obtained with the experimental results, this simple model establishes a linear relation between the crack length and the period of the mechanical wave. The associated damping ratio, calculated by identification to the Eq. 4, is slightly inferior to 1 characterizing an underdamped oscillator close to the critical damping. In other words, the mechanical wave is a periodic wave with a quick exponential damping which well defines an acoustic emission hit.

$$
\begin{cases}
\ddot{X} + 2\delta \cdot \dot{X} + \omega_0^2 \cdot X = 0 \text{ and } X(t) = A\mathrm{e}^{-\delta \cdot t}\cos(\omega \cdot t) \\
\omega_0 = \sqrt{\frac{k}{m}}, \omega = \omega_0\sqrt{1-\zeta^2} \text{ and } \zeta = \frac{\delta}{\omega_0} \\
k = \frac{48EI}{d^3}, I = \frac{d^4}{12} \text{ and } m = \rho\pi\frac{d^3}{4} \\
T = \frac{2\pi}{\omega} = \frac{1}{2}\sqrt{\frac{\rho\pi^3}{E(1-\zeta^2)}} \cdot d \Rightarrow \boxed{\lambda \approx 0.84\sqrt{\frac{E(1-\zeta^2)}{\rho\pi^3}} \cdot T} \\
\quad\Rightarrow \zeta \approx 0,9986
\end{cases}
$$

$$(5)$$

Furthermore, the initial energy of the generated mechanical wave can be calculated using the initial elastic potential energy of the harmonic oscillator E_p (Eq. 6). The amplitude A (i.e., the initial grain deflection) is calculated from the beam theory using the flexural strength σ of tungsten carbide which is about 340 ± 20 MPa [14]. The acoustic emission should represent a small part of this potential energy. Eventually, as for the experimental results, the calculation leads to a linear relation between the AE energy and the cube of the crack length. The share of the AE energy from the overall potential energy given by the factor β is about 4×10^{-8}.

$$
\begin{cases}
E_p = \frac{1}{2}k \cdot X^2(0) = \frac{1}{2}k \cdot A^2 \\
\text{with } A = \frac{Fd^3}{48EI} = \frac{F}{4Ed} = \frac{\pi\sigma}{16E} \cdot d \\
\Rightarrow E_p = \frac{(\pi\sigma)^2}{128E} \cdot d^3 \Rightarrow \boxed{E_{AE} \approx \beta\frac{(\pi\sigma)^2}{9.5E} \cdot \lambda^3} \text{ with } \beta \approx 4 \cdot 10^{-8}
\end{cases}
$$

$$(6)$$

Equations 5 and 6 do not present significant threshold values as in the empirical equations 3 and 4. The mechanical model presented here concerns a single grain. The cemented carbide WC–Co more complex polycrystalline microstructure induces these threshold values. For instance, as observed in previous studies, the transgranular crack occurrence decreases with the WC grain size which imposes a threshold.

5 Conclusions

The one-way scratch test performed on WC–Co contact generates a cohesive plastic wear volume that is well predicted knowing the cemented carbide hardness. On the wear track, the classical interfacial wear mechanisms observed in this material are retrieved here with cobalt depletion, intergranular cracks, grains plastic deformation, and grain cleavage. By an effect of solid lubrication, the friction coefficient is directly related to the amount of cobalt at the interface produced with finer microstructures. The major results of this study gather the characterization of the transgranular cracks, their identification using the acoustic emission technique, and the application of the classical beam theory and the simple harmonic motion equation:

– The transgranular cracks length are formed near the middle of a grain and are transversal to the sliding direction.
– The acoustic emission energy increases linearly with the cube of the crack length.
– The acoustic emission centroid frequency is a linear function of the source size, i.e., the crack length.

Declarations

References

1. Chermant, J.L., Osterstock, F.: Fracture toughness and fracture of WC–Co composites. J. Mater. Sci. **11**, 1939–1951 (1976)
2. Yahiaoui, M., Paris, J.-Y., Denape, J., Dourfaye, A.: Wear mechanisms of WC–Co drill bit inserts against alumina counterface under dry friction: Part 1-WC–Co inserts with homogenous binder phase content. Wear **48**, 245–256 (2015)
3. Beste, U., Hartzell, T., Engqvist, H., Axén, N.: Surface damage on cemented carbide rock-drill buttons. Wear **249**, 324–329 (2001)
4. Baranov, V., Kudryavtsev, E., Sarychev, G., Schavelin, V.: Acoustic Emission in Friction. Elsevier, Amsterdam (2007)
5. Hase, A., Mishina, H., Wada, M.: Correlation between features of acoustic emission signals and mechanical wear mechanisms. Wear **292–293**, 144–150 (2012)
6. Ferrer, C., Salas, F., Pascual, M., Orozco, J.: Discrete acoustic emission wavesduring stick-slip friction between steel samples. Tribol. Int. **43**, 1–6 (2010)
7. Chang, H., Han, E.H., Wang, J.Q., Ke, W.: Acoustic emission study of fatigue crackclosure of physical short and long cracks for aluminum alloy LY12CZ. Int. J. Fatigue **31**, 403–407 (2009)
8. Feng, P., Borghesani, P., Smith, W.A., Randall, R.B., Peng, Z.: A review on the relationships between acoustic emission, friction and wear in mechanical systems. Appl. Mech. Rev. **72**, 020801–020818 (2020)
9. Christensen, M., Wahnström, G., Lay, S., Allibert, C.H.: Quantitative analysis of WC grain shape in sintered WC–Co cemented carbides. Phys. Rev. Lett. **94**, 066105 (2005)
10. Milman, Y., Luyckx, S., Northrop, I.: Influence of temperature, grain size and cobalt content on the hardness of WC–Co alloys. Int. J. Refract. Metals Hard Mater. **17**, 39–44 (1999)
11. Yahiaoui, M., Chabert, F., Paris, J.-Y., Denape, J.: Friction, acoustic emission, and wear mechanisms of a PEKK polymer. Tribol. Int. **132**, 154–164 (2019)
12. Bradt, R.C., Hasselman, D.P.H., Munz, D., Sakai, M., Shevchenko, V.Y.: Fracture Mechanics of Ceramics: Fracture Fundamentals, High-Temperature Deformation, Damage, and Design. Springer, New York (1992)
13. Yang, K.-H., Kobayashi, A.S.: Dynamic fracture responses of alumina and two ceramic composites. J. Am. Ceram. Soc. **73**, 2309–2315 (1990)
14. Exner, H.E., Gurland, J.: A review of parameters influencing some mechanical properties of tungsten carbide–cobalt alloys. Powder Metall. **13**, 13–31 (1970)